$Na_2Te_3Mo_3O_{16}$: A New Molybdenum Tellurite with Second-Harmonic Generating and Pyroelectric Properties

Eun Ok Chi, Kang Min Ok, Yetta Porter, and P. Shiv Halasyamani*

Department of Chemistry and Center for Materials Chemistry, University of Houston, 136 Fleming Building, Houston, Texas 77204-5003

Received November 27, 2005. Revised Manuscript Received February 14, 2006

The synthesis, structure, and characterization of a new noncentrosymmetric molybdenum tellurite, $Na_2Te_3Mo_3O_{16}$, are reported. $Na_2Te_3Mo_3O_{16}$ crystallizes in the noncentrosymmetric monoclinic space group $I2$ (No. 5, cell choice 3) with $a = 7.3373(10)$ Å, $b = 11.2668(16)$ Å, $c = 8.2369(18)$ Å, and $\beta = 97.387(3)°$. The material exhibits a quasi-one-dimensional crystal structure, with each chain consisting of edge-shared MoO_6 octahedra that are connected by TeO_3 and TeO_4 polyhedra. The SHG efficiency of $Na_2Te_3Mo_3O_{16}$, using 1064 nm radiation, is approximately 500 × α-SiO_2 and is phase-matchable (type 1). The strong SHG efficiency is maintained up to the melting temperature. The maximum polarization is 0.189 $\mu C/cm^2$ at 25 kV/cm, and the pyroelectric coefficient (total effect), p, is -2.6 $\mu C/m^2$ K.

Introduction

Noncentrosymmetric (NCS) compounds exhibit many interesting and useful properties such as ferroelectricity, piezoelectricity, and second-order nonlinear optical behavior. With inorganic materials, the macroscopic acentricity is often a manifestation of the asymmetric coordination environments of the metal cations. The asymmetry is a necessary but not sufficient condition for producing crystallographic NCS. That is, the material may crystallize with the asymmetric units aligned in an inversion relationship, leading to overall crystallographic centrosymmetry. Recently, a variety of strategies has been put forth for designing new NCS materials.[1−6] We have focused on creating new NCS materials[7−11] by synthesizing oxides containing cations susceptible to second-order Jahn−Teller (SOJT) distortions.[12−18] The distortion can occur in two different types of cations, d^0 transition metals (Ti^{4+}, Nb^{5+}, Mo^{6+}, W^{6+}) and cations with stereoactive lone pairs (Se^{4+}, Sb^{3+}, Te^{4+}), and results in asymmetric coordination environments. With the octahedrally coordinated d^0 transition metals, SOJT effects occur when the empty d orbitals of the metal mix with the filled p orbitals of the ligands. In extended structures, this mixing results in a host of nearly degenerate electronic configurations that can be removed through the spontaneous distortion of the d^0 transition metal. The situation with the lone-pair cations is somewhat more complex. Historically, the original work of Sidgwick and Powell[19] followed by the valence shell electron pair repulsion (VSEPR) theory of Gillespie and Nyholm[20] attempted to rationalize the coordination geometry of the lone-pair cation. However, it was Orgel[21] who explained the structural distortion and polarization through the mixing of the metal cation s and p orbitals. Recently, this traditional view of metal cation s−p orbital mixing has been shown to be incomplete. Watson and Parker,[22,23] Lefebvre et al.,[24,25] Spaldin, Seshadri et al.,[26,27] and Mudring et al.[28] have shown that the oxide anion plays an important role in the lone-pair formation. Specifically, these researchers argue that the interaction of the s and p orbitals of the metal cation with the oxide anion p states is critical for lone-pair formation. Regardless of how

* To whom correspondence should be addressed. E-mail: psh@uh.edu. Phone: 713-743-3278. Fax: 713-743-0796.

(1) Bruce, D.; Wilkinson, A. P.; While, M. G.; Bertrand, J. A. *J. Solid State Chem.* **1996**, *125*, 228.
(2) Kepert, C. J.; Prior, T. J.; Rosseinsky, M. J. *J. Am. Chem. Soc.* **2000**, *122*, 5158.
(3) Maggard, P. A.; Stern, C. L.; Poeppelmeier, K. R. *J. Am. Chem. Soc.* **2001**, *123*, 7742.
(4) Welk, M. E.; Norquist, A. J.; Arnold, F. P.; Stern, C. L.; Poeppelmeier, K. R. *Inorg. Chem.* **2002**, *41*, 5119.
(5) Evans, O. R.; Lin, W. *Acc. Chem. Res.* **2002**, *35*, 511.
(6) Hwu, S.-J.; Ulutagay-Kartin, M.; Clayhold, J. A.; Mackay, R.; Wardojo, T. A.; O'Connor, C. J.; Kraweic, M. *J. Am. Chem. Soc.* **2002**, *124*, 12404.
(7) Halasyamani, P. S.; Poeppelmeier, K. R. *Chem. Mater.* **1998**, *10*, 2753.
(8) Porter, Y.; Ok, K. M.; Bhuvanesh, N. S. P.; Halasyamani, P. S. *Chem. Mater.* **2001**, *13*, 1910.
(9) Ok, K. M.; Bhuvanesh, N. S. P.; Halasyamani, P. S. *J. Solid State Chem.* **2001**, *161*, 57.
(10) Goodey, J.; Broussard, J.; Halasyamani, P. S. *Chem. Mater.* **2002**, *14*, 3174.
(11) Goodey, J.; Ok, K. M.; Broussard, J.; Hofmann, C.; Escobedo, F. V.; Halasyamani, P. S. *J. Solid State Chem.* **2003**, *175*, 3.
(12) Opik, U.; Pryce, M. H. L. *Proc. R. Soc. London, Ser. A* **1957**, *238*, 425.
(13) Bader, R. F. W. *Mol. Phys.* **1960**, *3*, 137.
(14) Bader, R. F. W. *Can. J. Chem.* **1962**, *40*, 1164.
(15) Pearson, R. G. *J. Am. Chem. Soc.* **1969**, *91*, 4947.
(16) Pearson, R. G. *J. Mol. Struct. (THEOCHEM)* **1983**, *103*, 25.
(17) Wheeler, R. A.; Whangbo, M.-H.; Hughbanks, T.; Hoffmann, R.; Burdett, J. K.; Albright, T. A. *J. Am. Chem. Soc.* **1986**, *108*, 2222.
(18) Kunz, M.; Brown, I. D. *J. Solid State Chem.* **1995**, *115*, 395.
(19) Sidgwick, N. V.; Powell, H. M. *Proc. R. Soc. London, Ser. A* **1940**, *176*, 153.
(20) Gillespie, R. J.; Nyholm, R. S. *Q. Rev., Chem. Soc.* **1957**, *11*, 339.
(21) Orgel, L. E. *J. Chem. Soc.* **1959**, 3815.
(22) Watson, G. W.; Parker, S. C. *J. Phys. Chem. B* **1999**, *103*, 1258.
(23) Watson, G. W.; Parker, S. C.; Kresse, G. *Phys. Rev. B* **1999**, *59*, 8481.
(24) Lefebvre, I.; Lannoo, M.; Allan, G.; Ibanez, A.; Fourcade, J.; Jumas, J. C. *Phys. Rev. Lett.* **1987**, *59*, 2471.
(25) Lefebvre, I.; Szymanski, M. A.; Olivier-Fourcade, J.; Jumas, J. C. *Phys. Rev. B.* **1998**, *58*, 1896.
(26) Seshadri, R.; Hill, N. A. *Chem. Mater.* **2001**, *13*, 2892.
(27) Waghmare, U. V.; Spaldin, N. A.; Kandpal, H. C.; Seshadri, R. *Phys. Rev. B* **2003**, *67*, 12511.
(28) Mudring, A.-V.; Rieger, F. *Inorg. Chem.* **2005**, *44*, 6240.

10.1021/cm052614e CCC: $33.50
Published on Web 03/28/2006

Table 1. Crystallographic Data for $Na_2Te_3Mo_3O_{16}$

formula	$Na_2Te_3Mo_3O_{16}$	T (°C)	293.0(2)
fw	972.60	λ (Å)	0.71073
cryst dimensions (mm^3)	$0.05 \times 0.08 \times 0.17$	ρ_{calcd} (g cm^{-3})	4.783
color, habit	colorless, block	μ (mm^{-1})	9.250
cryst syst	monoclinic	$2\theta_{max}$ (deg)	55.94
space group	*I*2 (No. 5)	no. of refln/collected/unique	2082/1404
a (Å)	7.3373(10)	abs corr	Ψ-scan
b (Å)	11.2668(16)	R(int)	0.0368
c (Å)	8.2369(18)	GOF	1.081
β (°)	97.387(3)	extinction coeff	0.0022(3)
V ($Å^3$)	675.3(2)	$R(F)^a$	0.0331
Z	2	$R_w(F_o^2)^b$	0.0886

[a] $R(F) = \sum||F_o| - |F_c||/\sum|F_o|$. [b] $R_w(F_o^2) = [\sum w(F_o^2 - F_c^2)^2/\sum w(F_o^2)^2]^{1/2}$.

Table 2. Selected Bond Distances (Å) for $Na_2Te_3Mo_3O_{16}$

Te(1)−O(1) × 2	1.906(7)	Mo(1)−O(3) × 2	2.213(7)	Na(1)−O(2) × 2	2.273(10)
Te(1)−O(2) × 2	2.043(7)	Mo(1)−O(5) × 2	1.942(7)	Na(1)−O(4) × 2	2.936(13)
Te(2)−O(2)	1.904(7)	Mo(1)−O(6) × 2	1.727(7)	Na(1)−O(7) × 2	2.973(14)
Te(2)−O(3)	1.884(7)	Mo(2)−O(1)	1.964(7)	Na(1)−O(8) × 2	2.811(10)
Te(2)−O(4)	1.859(6)	Mo(2)−O(3)	2.190(7)	Na(2)−O(4) × 2	2.492(8)
		Mo(2)−O(4)	2.197(7)	Na(2)−O(6) × 2	2.399(7)
		Mo(2)−O(6)	1.965(7)	Na(2)−O(8) × 2	2.422(11)
		Mo(2)−O(7)	1.711(7)		
		Mo(2)−O(8)	1.715(8)		

the lone pair is created, its structural consequences are profound, as the lone pair "pushes" the oxide ligands toward one side of the cation, resulting in a highly asymmetric coordination environment.

We have chosen to investigate the $Na^+-Te^{4+}-d^0-$oxide system, specifically, where the d^0 transition metal is Mo^{6+}, to couple the SOJT distortions of Mo^{6+} and Te^{4+} and thereby promote the formation of a new NCS material. With respect to the $A^+-Te^{4+}-d^0-$oxide system, a few materials have been reported. Zero-, one-, two-, and three-dimensional $A^+-Te^{4+}-M^{6+}-O$ (where $A^+ = Na^+$, K^+, Rb^+, Cs^+, NH_4^+; $M^{6+} = Mo^{6+}$, W^{6+}) phases are known.[10,29−32] Among these materials, $Na_2TeW_2O_9$, $A_2M_3TeO_{12}$ ($A = NH_4^+$, Rb^+, Cs^+; $M = Mo^{6+}$, W^{6+}), and $BaTeM_2O_9$ ($M = Mo^{6+}$, W^{6+})[33] are noncentrosymmetric and have large SHG responses. Our investigation of the Na−Te−Mo−oxide system resulted in the synthesis of a new quasi-one-dimensional noncentrosymmetric material, $Na_2Te_3Mo_3O_{16}$. The synthesis, structure, second-harmonic generating, and pyroelectric properties of this new material are reported.

Experimental Section

Syntheses. Single crystals of $Na_2Te_3Mo_3O_{16}$ were synthesized hydrothermally from a solution of Na_2TeO_3 (0.400 g, 1.8×10^{-3} mol, 99%, Aldrich), MoO_3 (0.520 g, 3.6×10^{-3} mol, 99.5%, Baker) and 1 mL of H_2O. The mixture was placed in a 23 mL Teflon lined autoclave, heated to 220 °C for 2 days, and cooled to room temperature at 6 °C h^{-1}. Colorless bar-shaped crystals, subsequently shown to be $Na_2Te_3Mo_3O_{16}$, were recovered by filtration in 80% yield on the basis of Te. Bulk $Na_2Te_3Mo_3O_{16}$ was synthesized by standard solid-state techniques. Stoichiometric amounts of Na_2TeO_3 (0.200 g, 0.9×10^{-3} mol), TeO_2 (0.2881 g, 1.8×10^{-3} mol, 99+%, Aldrich), and MoO_3 (0.3898 g, 2.7×10^{-3} mol) were ground and wrapped with gold foil and heated to 450 °C for 40 h with an intermittent regrinding.

Structure Determination. The structure of $Na_2Te_3Mo_3O_{16}$ was determined by standard crystallographic methods. A colorless bar-shaped crystal (dimensions $0.05 \times 0.08 \times 0.17$ mm^3) was glued on to a glass fiber and room-temperature intensity data were collected on a Siemens SMART diffractometer equipped with a 1 K CCD area detector using graphite monochromated Mo Kα radiation. A hemisphere of data was collected using a narrow-frame method with scan widths of 0.30° in omega and an exposure time of 30 s $frame^{-1}$. The first 50 frames were remeasured at the end of the data collection to monitor instrument and crystal stabilities. The maximum correction applied to the intensities was <1%. The data were integrated using the Siemens SAINT program,[34] with the intensities corrected for Lorentz, polarization, air absorption, and absorption attributable to the variation in the path length through the detector faceplate. ψ-scans were used for the absorption correction on the hemisphere of data. The data were solved and refined using SHELXS-97 and SHELXL-97, respectively.[35,36] All atoms were refined with anisotropic thermal parameters and converged for $I > 2\sigma(I)$. All calculations were performed using the WinGX-98 crystallographic software package.[37] Crystallographic data and selected bond distances for $Na_2Te_3Mo_3O_{16}$ are given in Tables 1 and 2, with additional details found in the Supporting Information. For the polycrystalline sample, X-ray powder diffraction data were recorded on a SCINTAG XDS2000 automated diffractometer with Cu Kα radiation. The experimental powder X-ray diffraction data are in good agreement with the calculated data based on the single-crystal model (see the Supporting Information).

Infrared and Raman Spectroscopy and Thermogravimetric Analysis. The infrared spectrum was recorded on a Matteson FTIR 5000 spectrometer. The sample was mixed with dry KBr and pressed into a pellet. The Raman spectrum was recorded at room temperature on a Digilab FTS 7000 spectrometer equipped with a germanium detector with the powder sample placed in a capillary tube. Excitation was provided by a Nd:YAG laser at a wavelength of 1064 nm, and the output laser power was 500 mW. The spectral resolution was about 4 cm^{-1}, and 200 scans were collected.

(29) Balraj, V.; Vidyasagar, K. *Inorg. Chem.* **1998**, *37*, 4764.
(30) Balraj, V.; Vidyasagar, K. *Inorg. Chem.* **1999**, *38*, 1394.
(31) Balraj, V.; Vidyasagar, K. *Inorg. Chem.* **1999**, *38*, 3458.
(32) Balraj, V.; Vidyasagar, K. *Inorg. Chem.* **1999**, *38*, 5809.
(33) Ra, H.-S.; Ok, K. M.; Halasyamani, P. S. *J. Am. Chem. Soc.* **2003**, *125*, 7764.
(34) *SAINT, Program for Area Detector Absorption Correction*, version 4.05; Siemens Analytical X-ray Instruments: Madison, WI, 1995.
(35) Sheldrick, G. M.; *SHELXS97, A Program for Automatic Solution of Crystal Structures*; University of Göttingen: Göttingen, Germany, 1997.
(36) Sheldrick, G. M.; *SHELXL97, A Program for Crystal Structure Refinement*; University of Göttingen: Göttingen, Germany, 1997.
(37) Farrugia, L. J. *J. Appl. Crystallogr.* **1999**, *32*, 837.

Thermogravimetric analysis was carried out on a TGA 2950 thermogravimetric analyzer (TA Instruments). The sample was placed in a platinum crucible and heated at a rate of 10 °C min^{-1} from room temperature to 900 °C under flowing air.

Second-Order Nonlinear Optical Measurements. Powder SHG measurements were performed on a modified Kurtz-NLO system[38] using 1064 nm radiation. A detailed description of the equipment and methodology used has been published elsewhere.[8,9] For the variable-temperature SHG measurements from room temperature to 500 °C, the sample stage was covered with a glass furnace. A wire type heating element was wrapped around the sample tube, and a variable autotransformer was used for temperature controlling. A K type thermocouple was positioned at the opposite side of the sample tube (o.d. = 3.5 mm) from the laser spot. Because the SHG efficiency has been shown to depend strongly on particle size, polycrystalline samples were ground and sieved into distinct particle size ranges. To make relevant comparisons with known SHG materials, we also ground and sieved crystalline SiO_2 and $LiNbO_3$ into the same particle size ranges. No index-matching fluid was used in any of the experiments.

Polarization Measurements. The polarization was measured on a Radiant Technologies RT66A ferroelectric test system with a TREK high-voltage amplifier between room temperature and 205 °C in a Delta 9023 environmental test chamber. The unclamped pyroelectric coefficient, defined as d*P*/d*T* (change in polarization with respect to the change in temperature), was determined by measuring the polarization as a function of temperature. The sample was a sintered $^1/_2$ in. diameter disk (>95% dense) approximately 0.6 mm thick. Gold paste was applied to both sides. The polarization was measured statically from room temperature to 205 °C in 10 °C increments, with an electric field of 25 kV/cm. The temperature was allowed to stabilize before the polarization was measured.

Results and Discussion

$Na_2Te_3Mo_3O_{16}$ exhibits a one-dimensional crystal structure consisting of MoO_6 octahedra connected to TeO_3 and TeO_4 polyhedra (see Figure 1a). The MoO_6 octahedra share edges and are observed as trimers (see Figure 1b). Connected to these octahedral trimers are the TeO_3 and TeO_4 groups. In connectivity terms, the structure may be written as $\{[TeO_{4/2}]^0\ 2[TeO_{2/2}O_{1/3}]^{+4/3}\ [MoO_{2/1}O_{2/2}O_{2/3}]^{-4/3}\ 2[MoO_{2/1}O_{3/2}O_{1/3}]^{-5/3}\}^{2-}$ with charge balance maintained by two Na^+ cations. The Mo−O and Te−O bond distances range from 1.711(7) to 2.213(7) Å and 1.859(6) to 2.043(7) Å, respectively. Bond valence calculations[39,40] resulted in values of 5.95 and 6.01 for Mo^{6+} and 4.10 and 3.88 for Te^{4+}. Both the Mo^{6+} and Te^{4+} cations are in asymmetric coordination environments attributable to SOJT effects. With the two unique Mo^{6+} cations, this effect is structurally manifested as a distortion toward an edge of the MoO_6 octahedron (see Figure 2). This edge, or C_2, distortion is the most commonly observed for Mo^{6+} cations.[41,42] In addition, using continuous shape measurers, we are able to calculate the magnitude of the off-center distortion.[43−47] For $Mo^{6+}(1)$ and $Mo^{6+}(2)$, these values are 0.165 and 0.103 $Å^2$, respectively, and are consistent with other octahedrally coordinated Mo^{6+} cations.[42] With the Te^{4+} cations, a lone pair is observed that results in an asymmetric coordination environment (see Figure 2). We can also calculate the dipole moment of the TeO_3 and TeO_4 polyhedra using a methodology described earlier.[48−50] This calculation results in values of 10.77 and 9.75 D for the TeO_3 and TeO_4 groups, respectively, and is consistent with earlier reported values.[50]

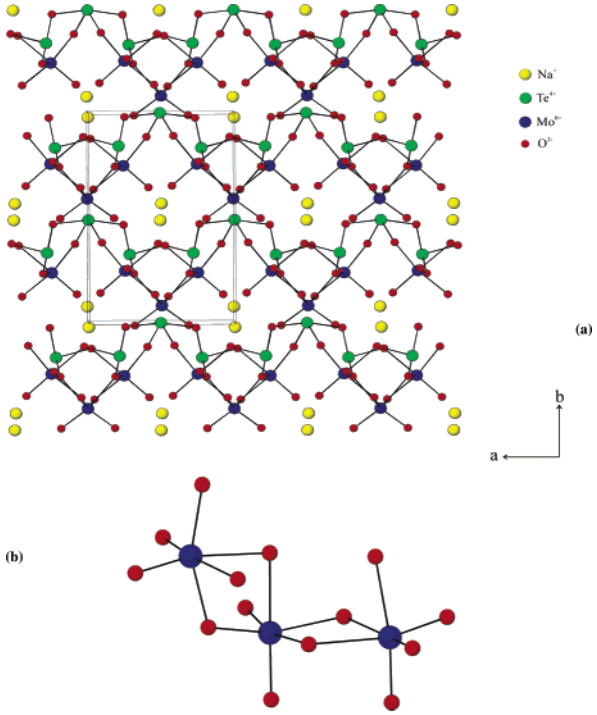

Figure 1. Ball-and-stick diagram of (a) $Na_2Te_3Mo_3O_{16}$ in the *ab* plane. Note that both the TeO_3 and TeO_4 polyhedra link the MoO_6 octahedra and (b) the edge-shared MoO_6 octahedral trimers.

The infrared and Raman spectra of $Na_2Te_3Mo_3O_{16}$ revealed Te−O, Mo−O, and Te−O−Mo vibrations between 400 and 1000 cm^{-1} (see Table 3). The Mo−O vibrations are observed between 450 and 570 cm^{-1} and 840−930 cm^{-1} in both the IR and Raman spectra. The bands occurring between 600 and 800 cm^{-1} may be assigned to Te−O and Te−O−Mo stretches. The vibrations are consistent with those previously published.[29,51,52] The thermal behavior of $Na_2Te_3Mo_3O_{16}$ was investigated using thermogravimetric analysis. The material melts at ~450 °C, and a single-step decomposition occurs above 700 °C. The TGA curve is available in the Supporting Information.

(38) Kurtz, S. K.; Perry, T. T. *J. Appl. Phys.* **1968**, *39*, 3798.
(39) Brown, I. D.; Altermatt, D. *Acta Crystallogr., Sect. B* **1985**, *41*, 244.
(40) Brese, N. E.; O'Keeffe, M. *Acta Crystallogr., Sect. B* **1991**, *47*, 192.
(41) Halasyamani, P. S. *Chem. Mater.* **2004**, *16*, 3586.
(42) Casanova, D.; Llunell, M.; Alemany, P.; Alvarez, S.; Ok, K. M.; Halasyamani, P. S. **2006**, submitted.
(43) Zabrodsky, H.; Peleg, S.; Avnir, D. *J. Am. Chem. Soc.* **1992**, *114*, 7843.
(44) Avnir, D.; Katzenelson, O.; Keinan, S.; Pinsky, M.; Pinto, Y.; Salomon, Y.; Zabrodsky, H. *Concepts in Chemistry: A Contemporary Challenge*; Research Studies Press Ltd.: Taunton, U.K., 1996.
(45) Alvarez, S.; Avnir, D.; Llunell, M.; Pinsky, M. *New J. Chem.* **2002**, *26*, 996.
(46) Llunell, M.; Casanova, D.; Cirera, J.; Bofill, J. M.; Alemany, P.; Alvarez, S.; Pinsky, M.; Avnir, D. *SHAPE Program*, version 1.1; Universitat de Barcelona: Barcelona, Spain, 2003.
(47) Alvarez, S.; Alemany, P.; Avnir, D. *Chem. Soc. Rev.* **2005**, *34*, 313.
(48) Maggard, P. A.; Nault, T. S.; Stern, C. L.; Poeppelmeier, K. R. *J. Solid State Chem.* **2003**, *175*, 25.
(49) Izumi, H. K.; Kirsch, J. E.; Stern, C. L.; Poeppelmeier, K. R. *Inorg. Chem.* **2005**, 44, 884.
(50) Ok, K. M.; Halasyamani, P. S. *Inorg. Chem.* **2004**, *44*, 3919.
(51) Bart, J. C. J.; Cariati, F.; Sgamellotti, A. *Inorg. Chim. Acta* **1979**, *36*, 105.
(52) Ok, K. M.; Halasyamani, P. S. *Inorg. Chem.* **2004**, *43*, 4248.

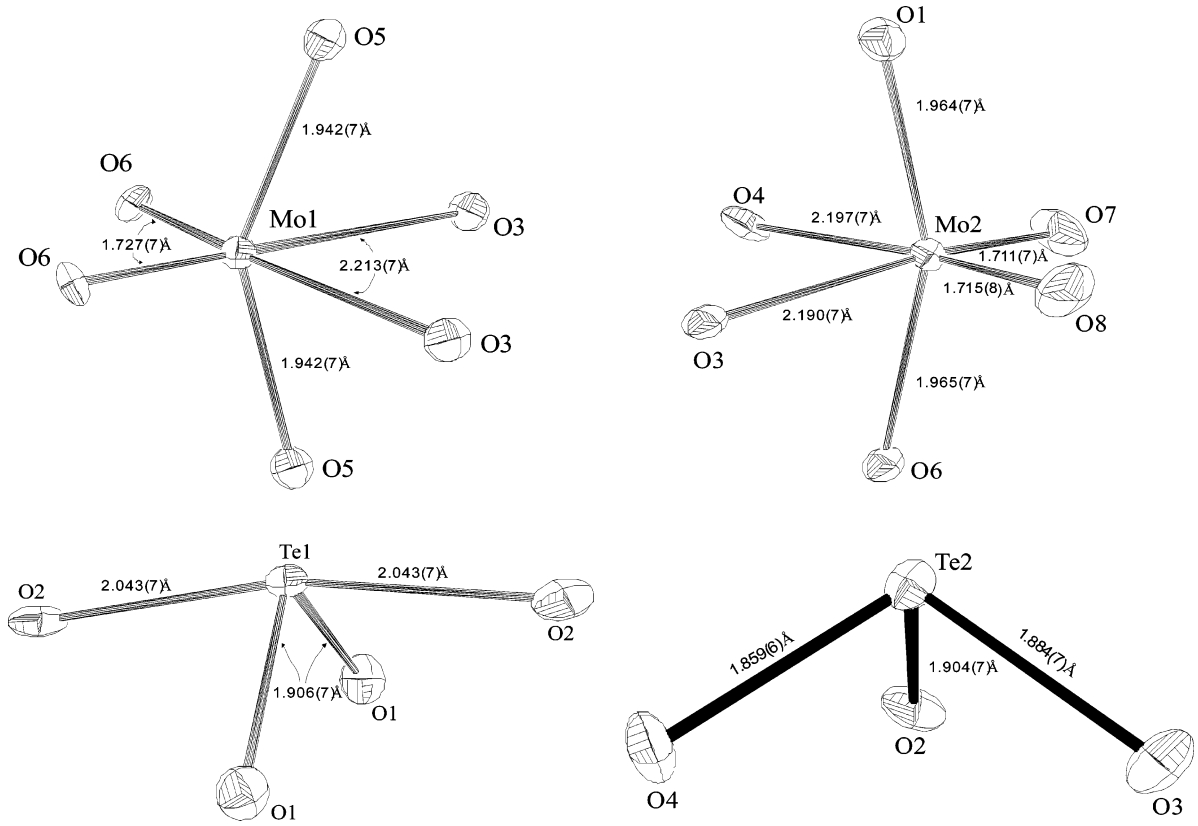

Figure 2. ORTEP (50% probability level ellipsoids) for the TeO_3, TeO_4, and MoO_6 polyhedra are shown. Note that the Te^{4+} cations are in asymmetric coordination environments attributable to their nonbonded electron pair, whereas the Mo^{6+} cation undergoes a local C_2 distortion (toward an edge), resulting in two short, two normal, and two long Mo−O bonds.

Table 3. Infrared and Raman Vibrations for $Na_2Te_3Mo_3O_{16}$

Mo−O	Te−O	Mo−O−Te
	IR (cm^{-1})	
922.77	793.56	678.34
903.01	767.53	600.72
881.31	684.61	
852.86	615.66	
754.51		
566.97		
513.45		
499.95		
458.01		
	Raman (cm^{-1})	
921.97	756.09	678.94
895.51	644.22	
867.97		
848.68		
756.09		
486.06		
457.06		

As $Na_2Te_3Mo_3O_{16}$ crystallizes in noncentrosymmetric space group *I*2, SHG measurements were performed. By sieving the powder in different particle sizes (20−120 μm), we determined that $Na_2Te_3Mo_3O_{16}$ is phase-matchable with an SHG efficiency of ∼500 × α-SiO_2. Once the phase-matching behavior has been determined and the SHG efficiency measured, the average NLO susceptibility, $\langle d_{eff}\rangle_{exp}$, can be estimated.[10] For phase-matchable materials

$$\langle d_{eff}\rangle_{exp} = \{7.98 \times 10^2[I^{2\omega}(Na_2Te_3Mo_3O_{16})/I^{2\omega}(LiNbO_3)]\}^{1/2}$$

where $I^{2\omega}(LiNbO_3) = 600$ (the SHG efficiency of $LiNbO_3$ compared to α-SiO_2). Because $I^{2\omega}(Na_2Te_3Mo_3O_{16}) = 500$, $\langle d_{eff}\rangle_{exp}(Na_2Te_3Mo_3O_{16}) = 25.8$ pm/V. The strong SHG response is not only attributable to the individual β(M−O)s but also to the asymmetric coordination environments of the MoO_6, TeO_3, and TeO_4 polyhedra. Using a model developed earlier, where the metal−oxygen bonds are treated as vectors and given specific hyperpolarizability values β(M−O), we were able to calculate $\langle d_{eff}\rangle$ for $Na_2Te_3Mo_3O_{16}$.[10,38,53] The β-(M−O)s for Mo−O and Te−O are 305 × 10^{-40} and 130 × 10^{-40} m^4/V, respectively.[10] Putting these values into the model results in a $\langle d_{eff}\rangle_{calcd}$ of 18.2 pm/V, which is in reasonable agreement with the experimentally determined value. Variable-temperature SHG measurements indicated that the doubling frequency remained constant until nearly the melting temperature. In addition, no thermal hysteresis was observed. Above 450 °C, $Na_2Te_3Mo_3O_{16}$ melts completely and the SHG intensity becomes zero. The variable-temperature SHG measurements are available in the Supporting Information. These measurements also indicate that $Na_2Te_3Mo_3O_{16}$ does not undergo a phase transition to a centrosymmetric structure before melting. As we will demonstrate, this observation has implications for the ferroelectric behavior, or lack thereof, of the material.

Space group *I*2 exhibits the correct symmetry for SHG as well as piezoelectricity.[54] We measured both the direct and converse piezoelectric effects. With the direct effect, a Berlincourt d_{33} meter was used, wherein a known force is applied to a sample and the resultant voltage is measured in pC/N. This measurement was done on a sintered and electrically poled disk ($^1/_2$ in. diameter, approximately 0.6 mm thick) of $Na_2Te_3Mo_3O_{16}$; however, the resultant voltage

(53) Bergman, J. G.; Crane, G. R. *J. Solid State Chem.* **1975**, *12*, 172.
(54) Nye, J. F. *Physical Properties of Crystals*; Oxford University Press: Oxford, U.K., 1957.

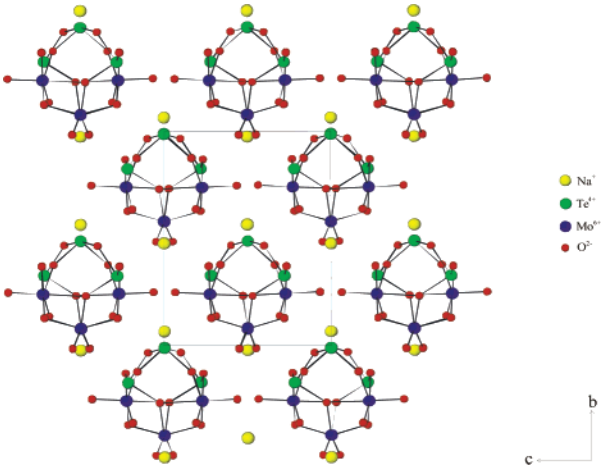

Figure 3. Ball-and-stick diagram of $Na_2Te_3Mo_3O_{16}$ in the *bc* plane. Note that the chains are staggered along the *b* axis.

was below the detection limit of the instrument, ~20 pC/N. With the converse effect, the application of a voltage results in the macroscopic deformation of the material. This macroscopic deformation occurs as a strain, i.e., a change in dimension $\Delta l/l$, parallel to the direction of the polarization. Again, we were unable to measure any deformation within the resolution of our instrument. Space group *I*2 is not only NCS but also polar, i.e., it possesses a permanent dipole moment, indicating possible ferroelectric behavior. In fact, the polar direction for this space group is defined to be along the [010] direction.[55] The nonbonded electron pair for the TeO_4 polyhedra is directed along the polar [010] direction. With the TeO_3 polyhedra, the lone pair points along the [101] and $[-10\bar{1}]$ directions, with a very small component along the [010] direction. Thus, the majority of the dipole moment attributable to the TeO_3 polyhedra cancels. With respect to Mo^{6+}, all of the MoO_6 octahedra contribute to the net moment. Both unique Mo^{6+} cations are displaced toward an edge of their oxide octahedron, polarizing each MoO_6 group. These polarizations are along the polar crystallographic *b* axis and, in combination with the TeO_3 and TeO_4 polyhedra, result in a net polarization along the [010] direction (see Figure 3). Although $Na_2Te_3Mo_3O_{16}$ is polar, it is not ferroelectric. That is, the permanent dipole moment along the [010] direction is not reversible, i.e., switchable, in the presence of an external electric field. In fact, polarization measurements using 25 kV/cm indicated an induced maximum polarization of only 0.189 $\mu C/cm^2$. The question of why the material is not ferroelectric is relevant. With any ferroelectric, the dipole moment needs to be reversible. In $Na_2Te_3Mo_3O_{16}$, this would include not only the dipole moment attributable to Mo^{6+}, but also Te^{4+}. In some instances it may be possible to reverse the polarization of the Mo^{6+} cation, i.e., move the cation from one side of its octahedron to the other in the presence of an external electric field. It is much more difficult to do this with a lone-pair cation such as Te^{4+}, because the required atomic displacements are far more severe. The lack of ferroelectric behavior is also consistent with our variable-temperature SHG measurements. As previously stated, the SHG efficiency remained nearly constant up to the melting point of the material, 450 °C. Thus, no phase change to a centrosymmetric nonpolar structure occurred. Although not common to all ferroelectrics, a phase-change to a centrosymmetric, nonpolar, paraelectric structure is often observed.

Although $Na_2Te_3Mo_3O_{16}$ is not ferroelectric, it is pyroelectric. Pyroelectricity is formally defined as the temperature dependence of the spontaneous polarization.[56,57] The pyroelectric coefficient $p = (\partial P_s/\partial T)_{E,S}$, where P_s is the spontaneous polarization and T is the temperature. The constraints are constant electric field, E, and constant elastic stress, S. Constant stress indicates the material is unclamped during the measurements and is free to thermally expand or contract. The primary pyroelectric coefficient is determined if the material is rigidly clamped during the measurement, whereas the secondary pyroelectric coefficient includes the additional change in polarization attributable to the volume change arising from the change in temperature. In practice, unclamped measurements give the sum of the primary and secondary coefficients.[56] We measured the unclamped, i.e., stress-free or total, pyroelectric coefficient, p, for $Na_2Te_3Mo_3O_{16}$. For pyroelectrics that exhibit ferroelectricity, the pyroelectric coefficient is determined by measuring the remanent polarization from the hysteresis loop at a variety of temperatures. For nonferroelectric pyroelectrics, such as $Na_2Te_3Mo_3O_{16}$, the hysteresis loop is linear; there is no remanent polarization. Thus, the pyroelectric coefficient is determined by measuring the polarization as a function of temperature at a specific electric field. With our instrumentation, the temperature range is between 25 and 205 °C, with an electric field of 25kV/cm. The polarization decreases with increasing temperature, and a first-order exponential function resulted in the best fit to the data (see the Supporting Information). The pyroelectric coefficient is approximately -2.6 $\mu C/m^2$ K at 40 °C. The magnitude of the pyroelectric coefficient for $Na_2Te_3Mo_3O_{16}$ is consistent with that of other nonferroelectric pyroelectrics. For example, nonferroelectric pyroelectrics such as ZnO and tourmaline have pyroelectric coefficients of -9.4 and -4.0 $\mu C/m^2$ K, respectively, whereas for ferroelectric pyroelectrics such as $BaTiO_3$ and $LiNbO_3$, the corresponding coefficients are -200 and -83 $\mu C/m^2$ K.[56]

Acknowledgment. We thank the Robert A. Welch Foundation for support. This work was also supported by the NSF Career Program through DMR-0092054, and by the NSF Chemical Bonding Center. E.O.C. thanks the Korea Science and Engineering Foundation (KOSEF) for postdoctoral support. P.S.H. is a Beckman Young Investigator.

Supporting Information Available: X-ray crystallographic file in CIF format, calculated and observed X-ray diffraction pattern, thermogravimetric analysis diagram, phase-matching curve, pyroelectric, and variable-temperature SHG data for $Na_2Te_3Mo_3O_{16}$. This material is available free of charge via the Internet at http://pubs.acs.org.

CM052614E

(55) Hahn, T., Ed. *International Tables for Crystallography*; 2nd ed.; D. Reidel Publishing Company: Dordrecht, The Netherlands, 1987; Vol. A.

(56) Lang, S. B.; Das-Gupta, D. K. In *Handbook of Advanced Electronic and Photonic Materials and Devices*; Nalwa, H. S., Ed.; Academic Press: San Francisco, 2001; Vol. 4, pp 1−55.

(57) Lang, S. B. *Phys. Today* **2005**, *58*, 31.